J Mol Model (2013) 19:5397–5406
DOI 10.1007/s00894-013-2033-3

ORIGINAL PAPER

A study of the solvent effect on the morphology of RDX crystal by molecular modeling method

Gang Chen · Mingzhu Xia · Wu Lei · Fengyun Wang · Xuedong Gong

Received: 25 July 2013 / Accepted: 9 October 2013 / Published online: 6 November 2013

Abstract Molecular dynamics simulations have been performed to investigate the effect of acetone solvent on the crystal morphology of RDX. The results show that the growth morphology of RDX crystal in vacuum is dominated by the (111), (020), (200), (002), and (210) faces using the BFDH laws, and (111) face is morphologically the most important. The analysis of surface structures of RDX crystal indicates that (020) face is non-polar, while (210), (111), (002), and (200) faces are polar among which (210) face has the strongest polarity. The interaction between acetone solvent and each RDX crystal face is different, and the order of binding energy on these surfaces is (210)>(111)>(002)>(200)>(020). The analysis of interactions among RDX and acetone molecules reveal that the system nonbond interactions are primary strong van der Waals and electrostatic interactions containing π-hole interactions, the weak hydrogen bond interactions are also existent. The effect of acetone on the growth of RDX crystal can be evaluated by comparing the binding energies of RDX crystalline faces. It can be predicted that compared to that in vacuum, in the process of RDX crystallization from acetone, the morphological importance of (210) face is increased more and (111) face is not the most important among RDX polar surfaces, while the non-polar (020) face probably disappears. The experimentally obtained RDX morphology grown from acetone is in agreement with the theoretical prediction.

Keywords Crystal morphology · Interfacial model · Molecular dynamics simulation · RDX · Solvent effect

G. Chen · M. Xia (✉) · W. Lei · F. Wang · X. Gong
Chemistry Department, Nanjing University of Science and Technology, Nanjing 210094, China
e-mail: icinjust@gmail.com

Introduction

RDX (cyclotrimethylene trinitramine, $C_3H_6N_6O_6$), as a high-performance energetic material, has been widely used in both civilian and military applications since it was synthesized [1]. RDX crystal primarily exits in α and β polymorphic forms at ambient conditions [2, 3]. Since α-RDX is quite a stable phase and β-RDX is highly unstable, α-RDX (default RDX hereinafter) is more valuable in practice. The sensitivity and packing density are crucial factors in affecting the performances of RDX product, because low sensitivity can increase stability and high packing density can promote explosive power [4, 5]. The research works have already shown that the crystal morphology of RDX plays an important role in determining packing density and sensitivity [6–9]. For instance, the spherical crystal shape has a higher packing density and smoother surfaces compared to other crystal shapes, such as the needle and plate. The crystal morphology is controlled not only by the internal structure but also the external factors such as super-saturation [10, 11], solvents [12, 13], and impurities [14, 15]. It is well-known that solvents have a great effect on the RDX crystal morphology [16–18]. It is, therefore, very important to understand the influence of solvents on the crystal morphology for controlling RDX crystallization process in order to achieve high packing density and low sensitivity.

Recently, molecular modeling has already been an important and effective tool to study the influence of specific solvents on the crystal morphology. Myerson et al. [19] provided a valid method to evaluate an additive effect on crystal growth with the binding energies as the additive-surface interaction by the aid of molecular modeling technique. The work of Ulrich et al. [20] proposed the Layer docking method to predict the crystal morphology in the presence of solvents by modeling the solid–liquid interface in the crystal growth process. Ter Horst et al. [17] considered the surface induced potential energy in the solid–liquid interface

as an adequate solvent effect parameter to predict the morphological importance of a crystal face. Molecular dynamics simulations were performed to study the effect of γ-butyrolactone solvent on the RDX (210) and (200) surfaces by the calculated surface induced potential energy. Duan et al. [21] constructed the HMX surfaces-acetone solvent interfacial model called a two-layer model. The modification morphology of HMX crystal in the presence of acetone was predicted by comparing the solvent-effected attachment energy which was calculated by employing molecular dynamics simulations.

Acetone is selected as the target solvent, because RDX has higher solubility in acetone solvent with the appropriate solubility ratio (d S/d T)/S compared with other common solvents, such as benzene, chloroform, ethanol, and diethyl ether. This is very suitable for the growth of high quality single RDX crystal from acetone [22]. The subject of our work is to understand the actions of acetone molecules on the RDX crystal surfaces at the molecular level by means of molecule modeling, and the purpose of the work is to provide some theoretical supports for RDX crystal morphology control technology. In this paper, the morphology of RDX crystal in vacuum was predicted by the laws of Bravais, Friedel, Donnay and Harker (BFDH) [23–25], the RDX surface-acetone solvent interfacial models were constructed and the molecular dynamics (MD) simulations were performed on these models, the interactions between RDX surfaces and acetone were analyzed and compared by the binding energy of each crystalline face, finally the RDX growth morphology in the presence of acetone was predicted and compared with the experimentally obtained RDX morphology.

Methods

Molecular dynamics simulations were run in the discover module which was implemented in the commercial software Accelrys Materials Studio (MS) [26]. All MD simulations were carried out in NVT ensemble with the COMPASS force field [27]. The RDX crystal morphology in vacuum was predicted using the BFDH laws in the polymorph module. The surface electrostatic potentials of RDX and acetone molecules on the 0.001 au were computed at the level of B3PW91 with 6-31G(d,p) basis set using the Gaussian 03 [28] and Surface Analysis Suite programs [29, 30].

The initial structure of RDX unit cell was derived from the experiment of Choi and Prince [3], which belongs to orthorhombic space group *PBCA* with eight molecules in the unit cell. The RDX unit cell structure and molecular configuration are shown in Fig. 1. From Fig. 1(a), there are eight irreducible RDX molecules in the unit cell with lattice parameters a=13.182 Å, b=11.574 Å, c=10.709 Å, $\alpha=\beta=\gamma=90°$. As seen from Fig. 1(b), the RDX molecule consists of three CH_2-N-NO_2 units arranged in a six-member ring, and the molecule conformation is the chair-AAE conformation, in which two nitro groups occupy axial positions (A) and the remaining nitro group is in the pseudo-equatorial positions (E).

The optimization of RDX crystal was performed in the COMPASS force field. The BFDH laws are used to predict crystal morphology in vacuum, which gives a list of the most probable crystal faces that appear in the external morphology. The crystal morphology and morphologically important (h k l) faces of the optimized RDX crystal in vacuum were determined by the BFDH laws. Then, the RDX crystal was cleaved along to the predicted (h k l) face with a depth of three unit cell. The crystal surface layer was constructed as a periodic superstructure of 3×3 unit cell. The chosen solvent was acetone with the dielectric constant ε_0 of 21 and density of 0.78 g/cm^3. A solvent layer containing 100 random distributed acetone molecules was constructed by the Amorphous Cell tool. Geometry optimization, followed by molecular dynamics simulations (100 ps with time step 1 fs at 303 K, using Andersen thermostat [31]) for the solvent layer

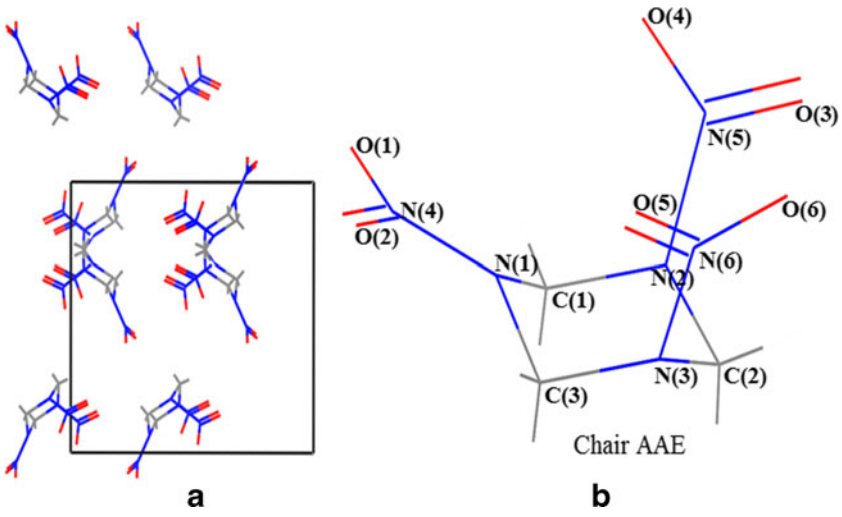

Fig. 1 The RDX unit cell structure (**a**) and molecule configuration (**b**)

was done to make acetone molecules uniformly distribute in the solvent layer. The RDX surface-acetone solvent interfacial models were built with the build tool in order to study the interactions between RDX crystalline faces and acetone. One part of the model was the crystal layer which was constrained along a, b, and c axis direction and the other was the acetone solvent layer which was placed on the (h k l) crystal face along c axis. A vacuum slab thickness of 50 Å was built above the solvent layer to eliminate the effect of additional free boundaries on the model. The schematic representation of RDX surface-acetone solvent interfacial model is shown in Fig. 2. The periodic boundary conditions were applied in all dimensions.

The interfacial models were firstly optimized by the energy minimization consisting of 5000 iteration steps. After that the MD simulations were carried out at 303 K which was the RDX crystallization temperature from acetone by application of Andersen thermostat [31]. Then, a period of 200 ps with time step 0.1 fs dynamics was run for equilibration stage. Subsequently, the production stage was performed with 200 ps during which data were collected every 200 time steps. For the potential-energy calculation, the atom based method was used to calculate van der Waals (vdW) interaction with a cut off distance of 12.5 Å and the Ewald summation method was applied to calculate the Coulomb interaction with the accuracy of 0.001 kcal·mol^{-1} [32]. The simulation details of MD are shown in Table 1.

Table 1 The simulation details of MD

Simulation parameter	Value	Simulation parameter	Value
Force field	COMPASS	Energy minimization	Smart minimizer
Ensemble	NVT	Nonbond	vdW, Coulomb
Thermostat	Andersen	Simulation temperature	303 K
Equilibration stage	200 ps	Production stage	200 ps
Time step	1 fs	Dielectric constant	21

Results and discussion

Choice of force field and equilibrium of system

The COMPASS force field is chosen to investigate the structure and properties of RDX crystal. There are two reasons, one is that the COMPASS force field is able to make accurate prediction of structural, conformational, and thermal physical properties for a broad range of compounds both in

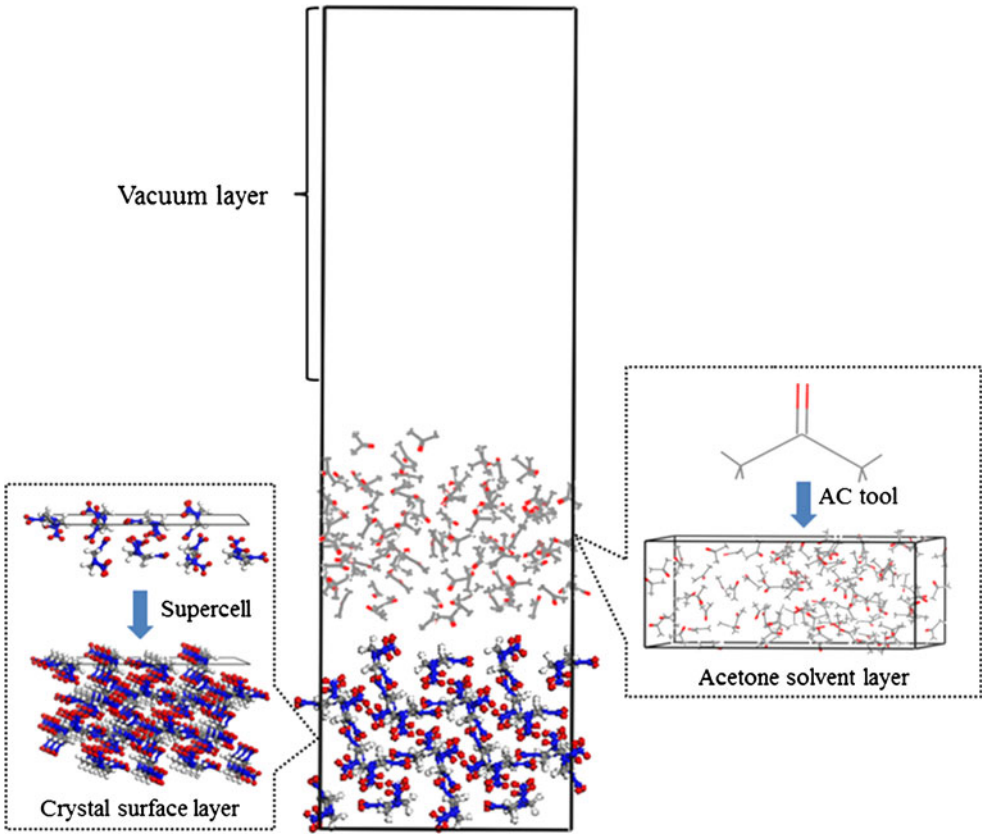

Fig. 2 The schematic representation of RDX surface-acetone solvent interfacial model

Table 2 Comparison of the optimized RDX unit cell parameters based on COMPASS force field with the experimental values

Lattice parameters						
Force field	a/Å	b/Å	c/Å	α/(deg)	β/(deg)	γ/(deg)
Exp.[3]	13.182	11.574	10.709	90	90	90
Compass	13.439(1.9 %)	11.275(2.6 %)	10.217(−1.4 %)	90	90	90

*() represents the deviation of RDX unit cell parameter between the optimized and experiment values

isolation and in condensed phases [33]. The other is that it has been successfully employed to model structures and properties of energetic materials, for example the cyclic nitramine compounds, HMX, TNAD and CL-20 [34–36]. The calculated results were consistent with their experimental values. RDX, as HMX homologues, also belongs to the cyclic nitramine explosive, so the COMPASS force field is applicable to simulate RDX crystal.

The reliability of the COMPASS force field can be checked by the accuracy of the calculated RDX cell unit and molecule structure parameters. The comparison of the optimized RDX unit cell parameters based on COMPASS force field with the experimental values is listed in Table 2. As can be seen, the optimized lattice parameters are in reasonable agreement with the experimental values, because the deviations of RDX lattice parameters between the optimized and experimental values are both less than 5 %. The comparison of the calculated structure parameters of the chair-AAE molecule conformation of RDX with the experimental values is listed in Table 3. From Table 3, the calculated structure parameters are also consistent with the experimental values, for which the deviations are both less than 5 %. Consequently, it is shown from the results that the COMPASS force field is really suitable to theoretical simulations for RDX crystal.

The equilibrium of system can be judged by two criteria for both the equilibrium of temperature and energy, simultaneously. When the fluctuation of temperature and energy are in the rage of 5–10 %, the equilibrium of the system is ascertained. Figure 3 shows that the fluctuation curves of temperature and energy of the RDX (210) surface-acetone solvent interfacial model for equilibration stage of 200 ps in the MD simulation. It can be observed that the system quickly equilibrates in less than 50 ps and then continues to fluctuate around the equilibrium state. The temperature equilibrates at the setting temperature of 303 K and fluctuates within ±15 K, when it reaches the equilibrium state. The fluctuation range of potential energy and nonbond energy are very small, and both energy deviations are less than ±1 %. Therefore, the system of RDX (210) face-acetone solvent interface has reached equilibrium states both in energy and temperature. Similarly, all other RDX crystal surface-acetone solvent interfacial models have been equilibrated according to the two criteria.

Table 3 Comparison of the calculated structure parameters of the chair-AAE molecule conformation of RDX with the experimental values

Structure parameters					
Bond (Å)	Exp.[3]	Cal.	Angle (deg)	Exp.[3]	Cal.
C(1)-N(1)	1.464	1.454(−0.7 %)	N(1)-C(1)-N(2)	107.843	110.594(2.6 %)
C(1)-N(2)	1.443	1.453(0.7 %)	C(1)-N(2)-C(2)	114.530	113.045(2.6 %)
C(2)-N(2)	1.467	1.449(−1.2 %)	N(2)-C(2)-N(3)	111.744	109.581(−1.9 %)
C(2)-N(3)	1.457	1.452(−0.3 %)	C(2)-N(3)-C(3)	114.840	110.632(−3.7 %)
C(3)-N(1)	1.450	1.452(0.1 %)	N(3)-C(3)-N(1)	108.354	108.787(0.4 %)
C(3)-N(3)	1.440	1.452(0.8 %)	C(3)-N(1)-C(1)	115.112	112.887(−1.9 %)
N(1)-N(4)	1.351	1.392(3.0 %)	C(1)-N(1)-N(4)	119.723	118.925(−0.7 %)
N(2)-N(5)	1.392	1.390(−0.1 %)	C(3)-N(1)-N(4)	120.892	118.725(−1.8 %)
N(3)-N(6)	1.398	1.396(−0.1 %)	C(1)-N(2)-N(5)	117.039	121.934(4.2 %)
N(4)-O(1)	1.209	1.212(0.2 %)	C(2)-N(2)-N(5)	116.652	121.050(3.8 %)
N(4)-O(2)	1.232	1.211(−1.7 %)	C(3)-N(3)-N(6)	115.607	116.654(0.9 %)
N(5)-O(3)	1.203	1.210(0.6 %)	C(2)-N(3)-N(6)	117.497	117.994(0.4 %)
N(5)-O(4)	1.207	1.212(0.4 %)	N(1)-N(4)-O(2)	117.790	117.252(−0.4 %)
N(6)-O(5)	1.201	1.212(0.9 %)	N(2)-N(5)-O(3)	117.170	117.681(0.4 %)
N(6)-O(6)	1.205	1.211(0.5 %)	N(3)-N(6)-O(6)	117.021	117.282(0.2 %)

*() represents the deviation of RDX unit cell parameter between the optimized and experiment values

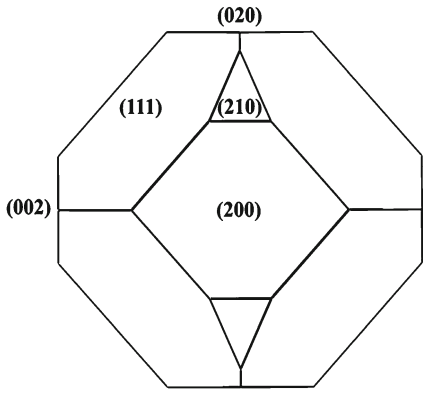

Fig. 3 The predicted growth morphology of RDX crystal in vacuum by using the BFDH laws

The production stage has been performed to run 200 ps after finishing the equilibrium task.

RDX crystal morphology and surface structures in vacuum

The growth morphology of RDX crystal in vacuum using the BFDH laws is shown in Fig. 4. The predicted results of RDX crystal are presented in Table 4.

From Fig. 4, the RDX crystal shape in vacuum is dominated by (111), (200) (002), (210), and (020) faces. From Table 3, (111) face has the largest percentage area which is almost about 74.1 % and the largest plane spacing (d_{111} = 6.75 Å). This indicates that (111) face is morphologically the most important growth face of RDX crystal. Face (200) is the second largest which has 12.9 % area percentage. The area percentage of (020) face is approximately 7.2 %. Both (002) and (210) faces have similar surface area, about 3.2 % and 2.6 %, respectively. The predicted results of RDX crystal in vacuum by the BFDH laws are also in accordance with the previous studies [16].

Table 4 The predicted results of RDX crystal in vacuum by using the BFDH laws

(h k l)	$d_{h\,k\,l}$ (Å)	Total facet area (%)
(210)	5.73	2.6
(002)	5.35	3.2
(020)	5.79	7.2
(200)	6.59	12.9
(111)	6.75	74.1

The molecular arrangements of (210), (111), (200), (002), and (020) faces of RDX crystal are displayed in Fig. 5. It can be found that (111) face is morphologically relatively smooth and other growth faces are rough because their molecular arrangements are uneven at the molecular level. The strong polar nitro groups (NO_2) are observed to be exposed at crystal surfaces except the (020) face exposes the non-polar methylene groups (CH_2). For (210) face, the exposed nitro groups are almost perpendicular to crystal surface and the number of the exposed oxygen atoms (O) is the largest, which is quite contributive to the formation of hydrogen bonds with surrounding solvent molecules. With respect to (002), (200), and (111) faces, the direction of exposed nitro groups are not perpendicular to crystal face and the quantity of exposed O atoms gradually becomes less. The polarity of crystal surface can be determined by the atoms which are exposed normal to the face [37]. From the view of crystal surface polarity, (210), (002), (200), and (111) faces are classified as polar due to the exposed NO_2 groups among which the polarity of (210) face is the strongest, whereas (020) face is considered as nonpolar because of the exposed CH_2 groups.

Binding energy

The equilibrium configurations of five different RDX surface-acetone solvent interfaces are displayed in Fig. 6. From this

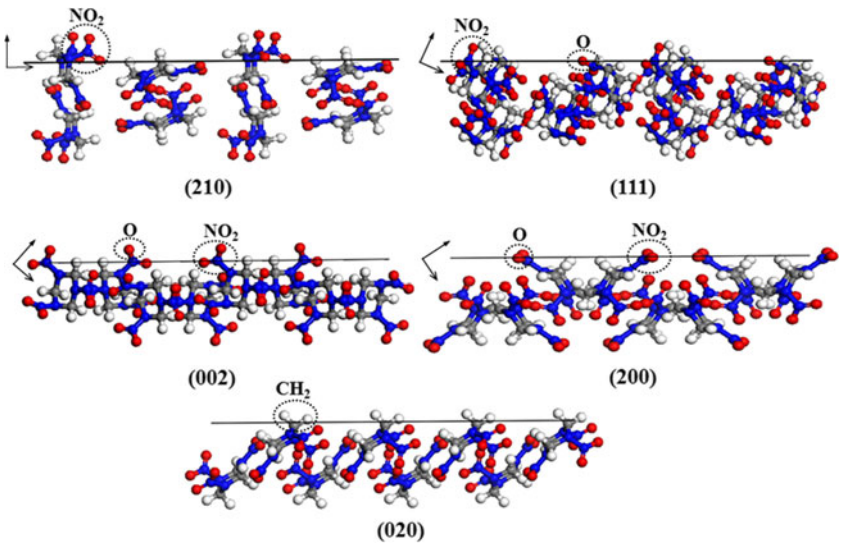

Fig. 4 The molecular arrangements of (210), (111), (002), (200), and (020) faces of RDX crystal

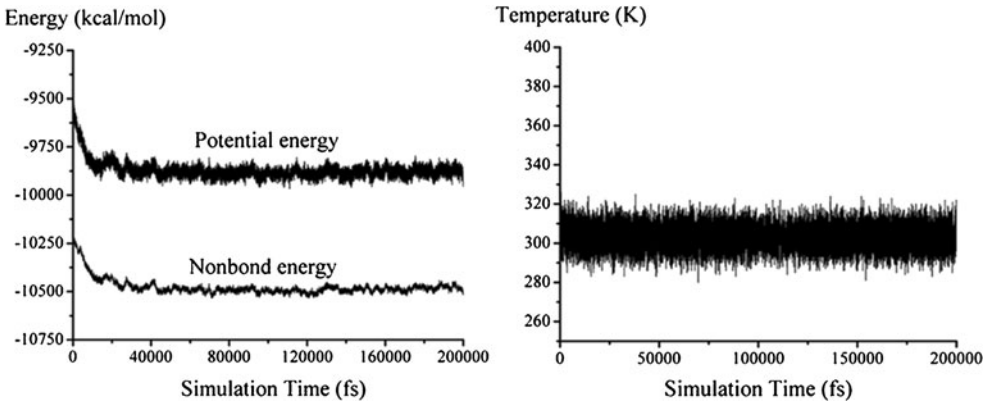

Fig. 5 Plot of energy and temperature vs simulation time for RDX (210) face-acetone solvent interface at 303 K

illustration, it can be seen that acetone molecules have already been in close contact with each crystalline surfaces and formed dense layers at surfaces, which implies that there exists strong interactions between RDX surfaces and acetone. The interaction energies between RDX surfaces and acetone can be calculated using the following equation.

$$E_{int} = E_{tot} - (E_{sur} + E_{sol}),$$

where E_{tot} is the average total single point energy of RDX surface-acetone solvent interfacial model, E_{sur} and E_{sol} is the average single point energy of RDX surface and acetone solvent layer, respectively.

The binding energy can accurately reflect the ability for solvents to interact with crystal faces, which is defined as the negative value of interaction energy, so

$$E_{binding} = -E_{int}.$$

The average binding energies of acetone molecules adsorbed on different RDX surfaces are tabulated in Table 5. From Table 5, it can be found that (210) face has the largest binding energy of 100.41 kcal·mol^{-1}, while (020) face has the least binding energy of 40.69 kcal·mol^{-1}. The order of binding energies on different RDX growth faces is as follows: (210)>(111)>(002)>(200)>(020). It shows that the polar faces of RDX crystal have larger binding energies compared with the nonpolar face. This can be explained that the polar solvents, such as acetone, preferentially interact with the polar faces, especially the strong polar faces [37, 38]. The larger the value of binding energy, the stronger the affinity capability of solvent with crystal face. It indicates that (210) face has the strongest capability to interact with acetone because it has the largest binding energy, followed by (111) face, then (002) and (200) faces whose binding energies are close, while the affinity capability of (020) face with acetone solvent is the weakest whose binding energy is the least.

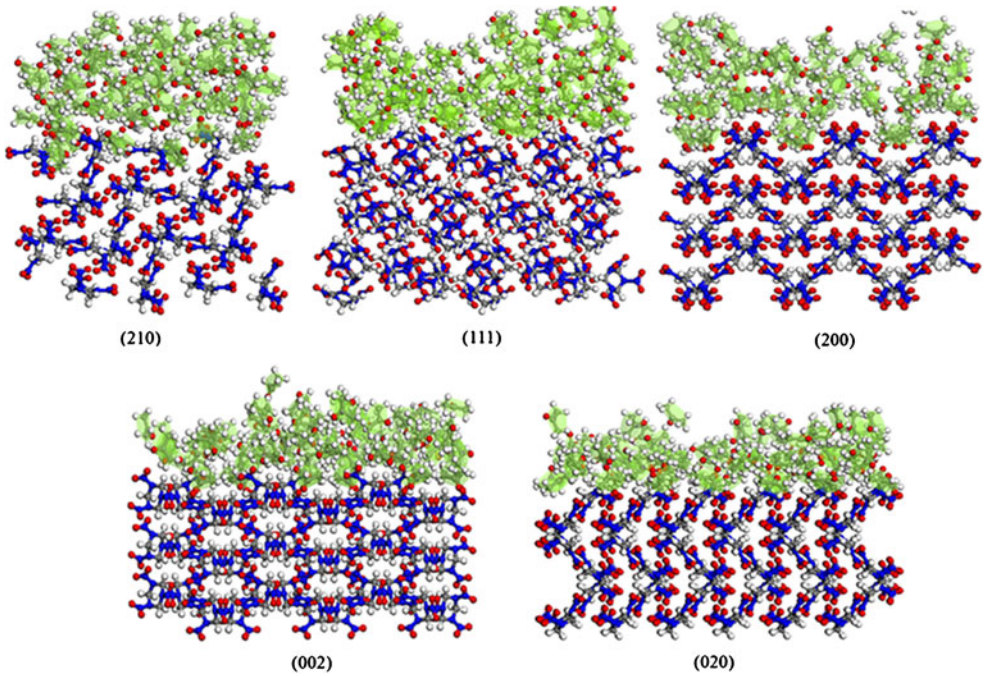

Fig. 6 The snapshot of equilibrium structures of RDX surfaces-acetone solvent interface at 303 K, which correspond to (210), (111), (200), (002), and (020) faces, respectively

Table 5 Calculated binding energies ($E_{binding}$) of acetone solvent adsorbed on five dominating surfaces of RDX crystal at 303 K

(*hkl*)	E (kcal·mol^{-1})				
	E_{tot}	E_{sur}	E_{sol}	E_{int}	$E_{binding}$[a]
(111)	−3155.44	−2555.46	−521.65	−78.33	78.33
(020)	−2474.72	−2255.03	−179.01	−40.68	40.69
(002)	−2624.24	−2328.17	−240.52	−55.55	55.54
(200)	−2534.22	−2243.12	−236.64	−54.46	54.45
(210)	−5316.09	−4473.29	−742.40	−100.40	100.41

[a] $E_{binding}=-E_{int}$

The molecular interaction analysis

The molecular interactions of acetone with RDX can be examined by analyzing the electrostatic potentials of RDX and acetone molecules. The surface electrostatic potentials of these molecules are shown in Figs. 7 and 8. From Fig. 7, the central regions of RDX molecule associated with the six ring are quite positive, while the negative regions are only limited on the peripheries of the molecule due to the lone pairs of nitro O atoms. From Fig. 8, the ketone O atom of acetone is quite negative owing to the lone pairs and π electron, the rest of the regions of the molecule are surrounded by positive potentials. For typical organic molecules, e.g., acetone, the negative potentials are stronger than the positive potentials, which should be attributed to the lone pair electrons on the more electronegative atom (e.g., O atom), but with respect to energetic compounds, the situation is overall different, e.g., RDX, which has three strong electron-attracting components, the nitro groups. These nitro groups are competing for the polarizable electronic charge of RDX molecule, as a result, each attracts less, whilst these electrons are considerably

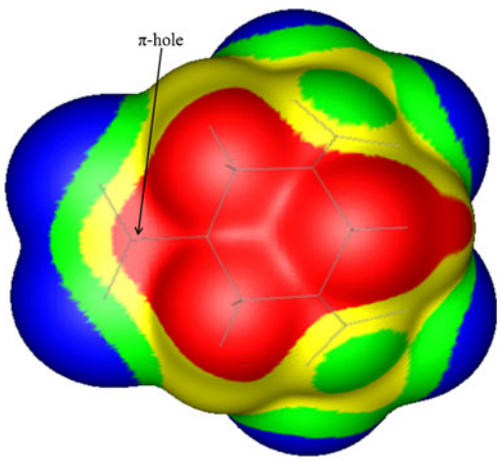

Fig. 7 The computed surface electrostatic potentials of RDX molecule on the 0.001 au. The color range, in kcal·mol^{-1}, are: *Red* greater than 29, *yellow* from 29 to 12, *green* between 12 and 0, *blue* less than 0

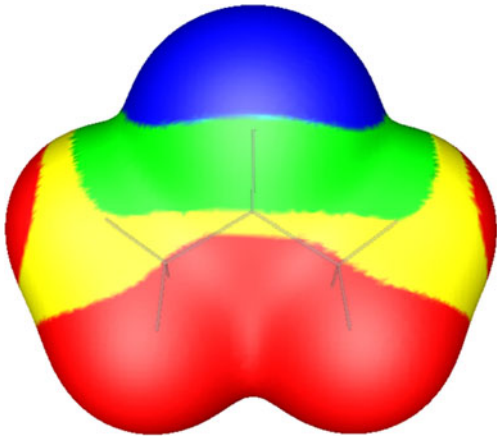

Fig. 8 The computed surface electrostatic potentials of acetone molecule on the 0.001 au. The color range, in kcal·mol^{-1}, are: *Red* greater than 6, *yellow* from 6 to 0, *green* between 0 and −22, *blue* less than −22

depleted by the strong electron-withdrawing ability of NO_2, so the positive potentials are quite stronger than the negative potentials, for which the most positive regions are near the nitro N atoms [39]. When these two molecules approach, through the negative potential sites interacting in a highly directional manner with positive sites, the strong electrostatic attracting interactions occur among RDX and acetone molecules. Moreover, the nitro N atoms of RDX can be regarded as the positive π-holes which are defined as the regions of low electronic density which are perpendicular to portions of a molecular framework [40]. The positive π-holes associated with nitro N atoms of RDX can electrostatically interact with the negative sites involving the lone pairs of ketone O atom in acetone. Consequently, the electrostatic interactions among RDX and acetone molecules include π-hole interactions.

The strongly positive potentials of RDX molecule associated with methylene hydrogen atoms identify possible hydrogen bond donors, whereas the strongly negative regions of acetone refer to the ketone O atom, indicating potential hydrogen bond acceptors. According to Desiraju's proposition, the weak hydrogen bond of C-H···O is defined for a maximum H···O distance of 2.8 Å, a maximum distance between C and O atoms of 4.0 Å, and a minimum C-H···O angle of 110° [41]. In terms of this criterion, it can be found that the C-H···O hydrogen bonds form at the RDX (210) surface-acetone solvent interface, as shown in Fig. 9. The hydrogen bonding geometry parameters listed in Fig. 8 show that the C-H···O interactions belong to the weak H-bonds. The pair correlation function is also used to investigate the nonbond interactions between solid and liquid structures, especially H-bonding interactions. The $g(r)_{O1-H2}\sim r$ and $g(r)_{O2-H1}\sim r$ curves of RDX (210) surface-acetone solvent interface are displayed in Fig. 10. The O and H atoms in the RDX molecule are named as O_1 and H_1, whereas O and H atoms in acetone molecules are named as O_2 and H_2. As seen from Fig. 9(a), the highest peak exists in the region of 2.1 ~

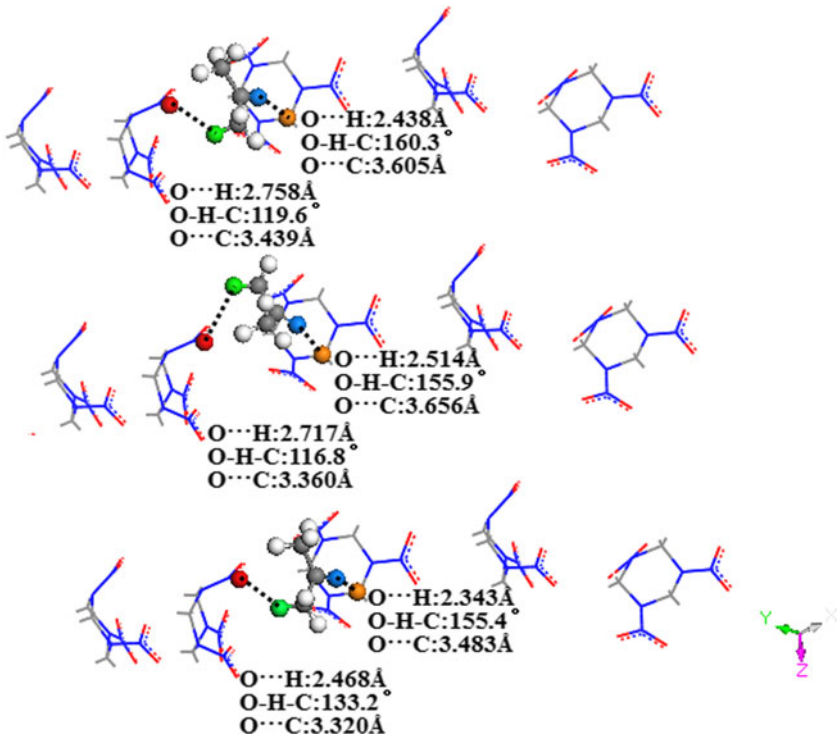

Fig. 9 The top view diagram of the formation of C-H···O hydrogen bonds at the RDX (210) surface-acetone solvent interface and these hydrogen bonding geometry parameters are given. It only keeps the first layer of (210) face for the intuitionistic display of hydrogen bonds. Color codes: *Red* ones represent the O atoms in RDX molecules; *Orange* ones represent the H atoms in RDX molecules; *Blue* ones represent the O ones in acetone molecules; *Green* ones represent the H atoms in acetone molecules

3.0 Å, indicating that the hydrogen bond exists between O_1 and H_2 atoms; it has some high peaks in the region of 3.0~8.0 Å, suggesting that the strong nonbond interactions exist between this atom pair. From Fig. 9(b), there is a high peak in the region of 2.1~3.0 Å, indicating that between O_2 and H_1 atoms hydrogen bonds form; some higher peaks exist in the region of 3.0~8.0 Å, implying that the strong vdW and electrostatic interactions exist between this atom pair.

It can be concluded that, the noncovalent interactions among RDX and acetone molecules are primarily strong vdW and electrostatic interactions including π-holes interactions, the weak hydrogen bond interactions also exist in the whole system.

The solvent effect on RDX morphology

During the process of crystallization from solution, solvents have an important influence on the crystal growth by the interactions between solvents and crystal faces. Due to the solvent-surface interactions, the solute molecules are hampered in depositing at crystal faces, in other words, the relative growth rates of corresponding surfaces are slowed and the growth of crystal faces are inhibited [12, 38], so ultimately the crystal morphology is affected which results from the relative growth rates of its faces in different directions [42]. If the solvent-surface interactions are stronger, it means that the growth of crystal face is slower and the influence of solvent on crystal growth is larger. Therefore, the effect of

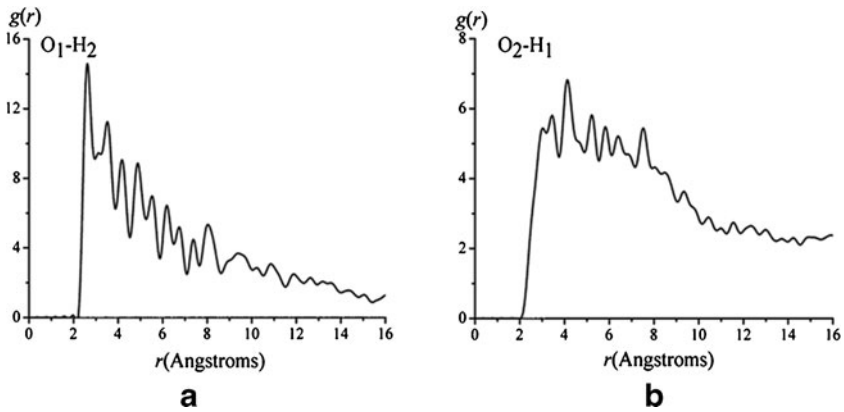

Fig. 10 The pair correlation functions $g(r)_{O1–H2}$ (**a**) and $g(r)_{O2–H1}$ (**b**) vs r of RDX (210) face-acetone solvent interface

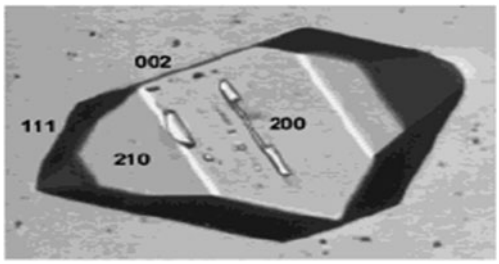

Fig. 11 The crystallization morphology of RDX crystal from acetone solvent [18]. (Copyright (2004) American Chemical Society)

acetone on the growth of RDX crystal can be evaluated by comparing the binding energy of each crystal face. Obviously, the growth of (210) face affected by acetone solvent is the strongest because it has the largest value of binding energy, while the solvent effect on (020) face is the lowest due to the weakest interaction. According to the binding energy, the effect of acetone on the RDX surfaces can be written as the following order: (210)>(111)>(002)>(200)>(020). Consequently, affected by acetone solvent, the relative growth rates of (210), (111), (002), and (200) faces is slow to a different extent among which (210) face relative growth rate becomes slow more remarkably, while the relative growth rate of (020) face becomes fast. Furthermore, the morphological importance of polar crystal face is increased in the polar solvent, while it is weakened in the non-polar solvent [35]. That is to say, if in the polar solvent, the morphological importance of RDX polar surfaces are increased, while the non-polar face is decreased, even probably disappears. Thus, based on these two points it can be predicted that, in the process of RDX crystal growth from acetone, the morphological importance of (210) face is increased more and (111) face is not the most important among polar surfaces of RDX crystal, while the non-polar (020) face probably disappears.

The RDX crystal morphology grown from acetone obtained from the cooling crystallization experiments is displayed in Fig. 11 [18]. It can be found that (210), (111), (002), and (200) faces which are of similar importance are revealed on the finally RDX crystal morphology, whereas (020) face disappears. The RDX crystallization experiment indicates that compared to that in vacuum, the morphological importance of RDX polar surfaces are increased, e.g., (210), (002), and (200) faces, except (111) face which is not the most important, and (020) face as a non-polar surface disappears in the acetone solvent. The experimental result is in agreement with the theoretical prediction.

Conclusions

In this work, we construct RDX surface-acetone solvent interfacial models, study the interactions between RDX crystal faces and acetone by performing the molecular dynamics simulations, and finally predict the effect of acetone solvent on the growth morphology of RDX crystal and compare it with the experimental results.

The growth morphology of RDX crystal in vacuum is dominated by the (111), (020), (200), (002), and (210) faces using the BFDH laws, in which (111) face is morphologically the most important. Analysis of surface structures of RDX growth faces show that (210), (002), (200), and (111) faces are polar among which (210) face has the strongest polarity, while (020) face is nonpolar. The ordering of binding energies on RDX crystal faces is: (210)>(111)>(002)>(200)>(020). The (210) face has the strongest capability to interact with acetone, followed by (111) face, then (002) and (200) faces whose binding energies are close, while the affinity capability of (020) face is the weakest. The analysis of pair correlation functions and molecular surface electrostatic potentials reveal that the nonbond interactions among RDX and acetone molecules are strong vdW and electrostatic interactions containing π-holes interactions, the weak hydrogen bonding interactions also exist in the whole system. Finally, it is predicted that in acetone solvent, compared to that in vacuum the morphological importance of (210) face is increased more and (111) face is not the most important among polar surfaces of RDX crystal, while (020) face as a nonpolar surface probably disappears. The crystallization morphology of RDX from acetone solvent shows that (210), (111), (002), and (200) faces were revealed on the finally RDX crystal morphology, whereas (020) face disappeared. The experimental results are in agreement with the theoretical predictions.

In a word, molecular dynamics simulation is a powerful tool to investigate the effect of acetone solvent on the crystal morphology of RDX. It can provide some theoretical support for RDX crystal morphology control technology, but it should be pointed that this theoretical prediction is qualitative and simple which only considers the solvent factor, because the temperature, stirring rate and super-saturation have equally important influence on the final morphology of RDX crystal.

Acknowledgments This work is supported by Institute of Industrial Chemistry, Nanjing University of Science & Technology.

References

1. Rogers J, Wright S, Lee P (1962) Physical and chemical properties of RDX and HMX. Holston Army Ammunition Plant
2. McCrone W (1950) Crystallographic data. 32. RDX (cyclotrimethylenetrinitramine). Anal Chem 22(7):954–955
3. Choi CS, Prince E (1972) The crystal structure of cyclotrimethylenetrinitramine. Acta Crystallogr B Struct Crystallogr Cryst Chem 28(9):2857–2862

4. Doherty RM, Watt DS (2008) Relationship between RDX properties and sensitivity. Propellants Explos Pyrotech 33(1):4–13. doi:10.1002/prep.200800201
5. Van der Heijden A, Ter Horst J, Kendrick J, Kim KJ, Krober H, Simon F (2005) Crysatllization. In: Teipel U (ed) Energetic materials. Wiley, Weinheim, pp 53–157
6. van der Heijden AE, Creyghton YL, Marino E, Bouma RH, Scholtes GJ, Duvalois W, Roelands MC (2008) Energetic materials: crystallization, characterization and insensitive plastic bonded explosives. Propellants Explos Pyrotech 33(1):25–32
7. Spyckerelle C, Eck G, Sjöberg P, Amnéus AM (2008) Reduced sensitivity RDX obtained from Bachmann RDX. Propellants Explos Pyrotech 33(1):14–19
8. Roberts CW, Hira SM, Mason BP, Strouse GF, Stoltz CA (2011) Controlling RDX explosive crystallite morphology and inclusion content via simple ultrasonic agitation and solvent evaporation. CrystEngComm 13(4):1074–1076
9. Stoltz C, Mason BP, Roberts C, Hira S, Strouse G (2012) Sonocrystallization as a tool for controlling crystalline explosivemorphology and inclusion content. In: AIP Conference Proceedings, p 641
10. Lu JJ, Ulrich J (2005) The influence of supersaturation on crystal morphology–experimental and theoretical study. Cryst Res Technol 40(9):839–846
11. Ma M, Ye W, Wang X-X (2008) Effect of supersaturation on the morphology of hydroxyapatite crystals deposited by electrochemical deposition on titanium. Mater Lett 62(23):3875–3877
12. Lahav M, Leiserowitz L (2001) The effect of solvent on crystal growth and morphology. Chem Eng Sci 56(7):2245–2253
13. Bhat MN, Dharmaprakash S (2002) Effect of solvents on the growth morphology and physical characteristics of nonlinear optical γ-glycine crystals. J Cryst Growth 242(1):245–252
14. Siegfried MJ, Choi K-S (2006) Elucidating the effect of additives on the growth and stability of Cu2O surfaces via shape transformation of pre-grown crystals. J Am Chem Soc 128(32):10356–10357
15. Thompson C, Davies MC, Roberts CJ, Tendler SJ, Wilkinson MJ (2004) The effects of additives on the growth and morphology of paracetamol (acetaminophen) crystals. Int J Phar 280(1):137–150
16. Ter Horst J, Geertman R, Van der Heijden A, Van Rosmalen G (1999) The influence of a solvent on the crystal morphology of RDX. J Cryst Growth 198:773–779
17. Ter Horst J, Geertman R, Van Rosmalen G (2001) The effect of solvent on crystal morphology. J Cryst Growth 230(1):277–284
18. van der Heijden A, Bouma RH (2004) Crystallization and characterization of RDX, HMX, and CL-20. Cryst Growth Des 4(5):999–1007
19. Myerson AS, Jang SM (1995) A comparison of binding energy and metastable zone width for adipic acid with various additives. J Cryst Growth 156(4):459–466
20. Schmidt C, Yürüdü C, Wachsmuth A, Ulrich J (2011) Modeling the morphology of benzoic acid crystals grown from aqueous solution. CrystEngComm 13(4):1159–1169
21. Duan X, Wei C, Liu Y, Pei C (2010) A molecular dynamics simulation of solvent effects on the crystal morphology of HMX. J Hazard Mater 174(1):175–180
22. Halfpenny P, Roberts K, Sherwood J (1984) Dislocations in energetic materials: IV. The crystal growth and perfection of cyclotrimethylene trinitramine (RDX). J Cryst Growth 69(1):73–81
23. Bravais A, de Beaumont LÉ (1866) Etudes cristallographiques: Mémoire sur les systèmes formés par des points distribués régulièrement sur un plan ou dans l'espace. Gauthiers-Villars
24. Friedel M (1907) Etudes sur la loi de Bravais. Bull Soc Fr Mineral 30: 326–455
25. Donnay J, Harker D (1937) A new law of crystal morphology extending the law of Bravais. Am Mineral 22(5):446–467
26. Materials Studio 4.0 (2007) Discover/Accelrys, San Diego, CA
27. Sun H (1998) COMPASS: an ab initio force-field optimized for condensed-phase applications overview with details on alkane and benzene compounds. J Phys Chem B 102(38):7338–7364
28. Frisch MJ, Trucks GW, Schlegel HB (2004) Gaussian 03. Gaussian, Inc., Wallingford, CT
29. Bulat FA, Toro-Labble A (unpublished) WFA: a suite of programs to analyse wavefunctions
30. Bulat FA, Toro-Labbé A, Brinck T, Murray JS, Politzer P (2010) Quantitative analysis of molecular surfaces: areas, volumes, electrostatic potentials and average local ionization energies. J Mol Model 16(11):1679–1691
31. Andersen HC (1980) Molecular dynamics simulations at constant pressure and/or temperature. J Chem Phys 72(4):2384
32. Ewald P (1921) Evaluation of optical and electrostatic lattice potentials. Ann Phys 64:253–287
33. Bunte SW, Sun H (2000) Molecular modeling of energetic materials: the parameterization and validation of nitrate esters in the COMPASS force field. J Phys Chem B 104(11):2477–2489
34. Xiao J, Fang G, Ji G, Xiao H (2005) Simulation investigations in the binding energy and mechanical properties of HMX-based polymer-bonded explosives. Chin Sci Bull 50(1):21–26
35. Qiu L, Xiao H-M, Zhu W-H, Xiao J-J, Zhu W (2006) Ab initio and molecular dynamics studies of crystalline TNAD (trans-1, 4, 5, 8-tetranitro-1, 4, 5, 8-tetraazadecalin). J Phys Chem B 110(22): 10651–10661
36. Xu X-J, Xiao H-M, Xiao J-J, Zhu W, Huang H, Li J-S (2006) Molecular dynamics simulations for Pure ε-CL-20 and ε-CL-20-based PBXs. J Phys Chem B 110(14):7203–7207
37. Berkovitch-Yellin Z (1985) Toward an ab initio derivation of crystal morphology. J Am Chem Soc 107(26):8239–8253
38. Stoica C, Verwer P, Meekes H, Van Hoof P, Kaspersen F, Vlieg E (2004) Understanding the effect of a solvent on the crystal habit. Cryst Growth Des 4(4):765–768
39. Murray JS, Concha MC, Politzer P (2009) Links between surface electrostatic potentials of energetic molecules, impact sensitivities and C–NO2/N–NO2 bond dissociation energies. Mol Phys 107(1):89–97
40. Murray JS, Lane P, Clark T, Riley KE, Politzer P (2012) σ-Holes, π-holes and electrostatically-driven interactions. J Mol Model 18(2): 541–548
41. Desiraju GR (2002) Hydrogen bridges in crystal engineering: interactions without borders. Acc Chem Res 35(7):565–573
42. Hartman P, Bennema P (1980) The attachment energy as a habit controlling factor: I. Theoretical considerations. J Cryst Growth 49(1):145–156